Biomechanics and Modeling in Mechanobiology
https://doi.org/10.1007/s10237-018-1010-2

ORIGINAL PAPER

A hybrid computational model for collective cell durotaxis

Jorge Escribano[1] · Raimon Sunyer[2,5] · María Teresa Sánchez[3] · Xavier Trepat[2,4,5,6] · Pere Roca-Cusachs[2,4] · José Manuel García-Aznar[1]

Received: 13 September 2017 / Accepted: 17 February 2018

Abstract
Collective cell migration is regulated by a complex set of mechanical interactions and cellular mechanisms. Collective migration emerges from mechanisms occurring at single cell level, involving processes like contraction, polymerization and depolymerization, of cell–cell interactions and of cell–substrate adhesion. Here, we present a computational framework which simulates the dynamics of this emergent behavior conditioned by substrates with stiffness gradients. The computational model reproduces the cell's ability to move toward the stiffer part of the substrate, process known as durotaxis. It combines the continuous formulation of truss elements and a particle-based approach to simulate the dynamics of cell–matrix adhesions and cell–cell interactions. Using this hybrid approach, researchers can quickly create a quantitative model to understand the regulatory role of different mechanical conditions on the dynamics of collective cell migration. Our model shows that durotaxis occurs due to the ability of cells to deform the substrate more in the part of lower stiffness than in the stiffer part. This effect explains why cell collective movement is more effective than single cell movement in stiffness gradient conditions. In addition, we numerically evaluate how gradient stiffness properties, cell monolayer size and force transmission between cells and extracellular matrix are crucial in regulating durotaxis.

Keywords Mechanics of cell migration · Stiffness gradients · Durotaxis · Cell contractility · Hybrid modeling approach · Collective cell motion

1 Introduction

Cell migration is crucial in a great number of biological processes, such as angiogenesis, wound healing, and cancer metastasis (Martin 1997; Yang and Weinberg 2008; Aman and Piotrowski 2010). In these processes, cell movement is determined by a complex assessment of environmental cues that include soluble factors, extracellular matrix (ECM) composition, anisotropy, and stiffness. Gradients related to these different cues might result in directional migration (Hartman et al. 2016). The most studied condition of directional cell migration is chemotaxis, which is the ability of cells to follow a gradient of soluble chemical cues (Roca-Cusachs et al. 2013; Majumdar et al. 2014; Moreno-Arotzena et al. 2015; Sunyer et al. 2016). It is also known that cells are able to sense and respond to the mechanical properties of their surrounding environment. Cell morphology and motility (Cherry and Adler 2000; Collins et al. 2000; Jia et al. 2015) are critically influenced by ECM stiffness. Cells placed in substrates with a spatial stiffness gradient move toward the stiffer part. This process is known as durotaxis, and it is implicated in development, fibrosis, and cancer (Ulrich et al. 2009; Liu et al. 2010; Sunyer et al. 2016).

The mechanisms guiding single cell migration in 2D are well understood, and they could be applied to collective migration. However, collective cell motility is not just

Electronic supplementary material The online version of this article (https://doi.org/10.1007/s10237-018-1010-2) contains supplementary material, which is available to authorized users.

✉ José Manuel García-Aznar
jmgaraz@unizar.es

1 University of Zaragoza, Zaragoza, Spain

2 Institute for Bioengineering of Catalonia (IBEC), The Barcelona Institute for Science and Technology (BIST), Barcelona, Spain

3 Centro Universitario de la Defensa, Zaragoza, Spain

4 University of Barcelona, Barcelona, Spain

5 Center for Networked Biomedical Research on Bioengineering, Biomaterials and Nanomedicine (CIBER-BBN), Barcelona, Spain

6 Institució Catalana de Recerca i Estudis Avançats (ICREA), Barcelona, Spain

Published online: 02 March 2018

the outcome of several cells moving independently. Collective movement also involves integration of guiding signals between cells in order to maintain the migration of cells as a group (Rørth 2011; Haeger et al. 2015). Cells move together in a coordinated way with a behavior that cannot be seen in individual cells. Recently, Merkher and Weihs (2017) observed how single cells exhibit less invasiveness when they are isolated than when they are surrounded by other cells. To understand how this collective behavior emerges is a current research topic that has been thoughtfully investigated (Mayor and Carmona-Fontaine 2010; Méhes and Vicsek 2014; Camley and Rappel 2017).

In order to understand the mechanism guiding both single and collective cell migration, computational modeling has been a powerful tool over these last years. Models can help us to determine whether a mechanism would be feasible and to make predictions that can be tested in experiments. They allow us to have much more control over any proposed mechanism, which we rarely have on experiments.

During the last few years there have been many attempts to model cell collective behavior and motility in order to obtain a deeper insight of the mechanisms that regulate this process and to understand how cells interact with each other to produce this collective behavior. Rappel et al. (Camley and Rappel 2017) have presented an interesting review of different works focusing on collective motility. In their work, they have divided the models into three main groups based on the number of cells that they have simulated: motion in micropatterned substrates, chemotaxis, and cell sheet models. Leong (2013) studied the dynamics of a pair of cells using a dissipative particle dynamics model that takes into account the acto-myosin forcing, viscous dissipation, and cortical tension. Later, Camley et al. (2014) simulated the same effect using the phase field model, including cell nucleus and polarity and considering the forces between the substrate and the other cell. Kulawiak et al. (2016) also used a computational phase field model of collective cell motility that includes the mechanics of cell shape and a minimal chemical model for CIL (contact inhibition for locomotion). They simulated a large number of cell–cell collisions on narrow micropatterned stripes, with the aim to probe which properties in the cell–cell interactions are responsible for the different outcomes.

There are different numerical approaches to simulate large amounts of cells: cellular Potts models can simulate cells in large confluent sheets (Kabla 2012), whereas vertex models are often used to simulate collective cell behavior in monolayer sheets. Both models could integrate feedback mechanisms between cell migration and motile forces. Hybrid models have also been used to predict the morphology of epithelial cells moving collectively (Gonzalez-Valverde and Garcia-Aznar 2017). Lin et al. (2016) have used a vertex model to study the effect on cancer cell invasion on the collective dynamics of a tumor monolayer. Peng et al. (2017) presented a two-scale moving boundary model of cancer invasion. Particle-based methods (Sepúlveda et al. 2013) and continuum approaches (Tambe et al. 2011; Cochet-Escartin et al. 2014) have also been used to model monolayer expansion. In chemotaxis different behavior between single and collective migration has also been reported and different models have been used to simulate this phenomenon (Theveneau et al. 2010; Malet-Engra et al. 2015).

Different cell-based models have been used to simulate large cell populations behavior in different scenarios: growing monolayers (Drasdo and Hoehme 2012), epithelial monolayers in tumor initiation stages and progression (Vermolen et al. 2015), wound contraction where the immune reaction, fibroblasts, and myofibroblasts are considered (Boon et al. 2016). Vermolen et al. (2016) used a cell-based model for epithelial wound healing that incorporates processes like cell proliferation and death, cell–cell contacts, random walk, chemotaxis, paralysation of constituent cells by pathogen-secreted lactates. Chen et al. (2017) used this kind of models to describe cell migration in nonisotropic fibrin networks around pancreatic tumor islets.

Models simulating durotaxis are not usual in the literature, and most of them correspond to single cell motion in 2D surfaces. Different approaches have been used to model single cell durotaxis. Stefanoni et al. (2011) proposed a 2D approach based on Langevin equation with some modifications to consider mechanical properties of the substrate to simulate single cell paths. Dokukina and Gracheva (2010) developed a model of a fibroblast with viscoelastic behavior using a Delaunay triangulation. Allena et al. (2016) used the previous mentioned cellular Potts model to reproduce single cell migration over flat substrates with different rigidity. More recently, Novikova et al. (2017) used a random walk model varying persistence time with substrate rigidity. Kim et al. (2015) built a force-based computational model in order to predict the cell invasion into a 3D ECM in response to chemotaxis and durotaxis cues. Collective durotaxis was studied previously by the same authors of this paper (Sunyer et al. 2016). In that work, it was observed how emergent collective behavior is more efficient than single cell behavior. A discrete clutch model which was able to predict experimental results was proposed.

Durotaxis in this model emerges as a consequence of a force balance. The combination of cell–cell interactions with a spatial–temporal analysis of discrete cell–ECM adhesions allows the system to respond to mechanical changes in the substrate. The model contains a monolayer formed by several discrete cells. Cells are bound to each other by cadherin proteins and each cell contracts and polymerizes. They also adhere to the extracellular matrix through adhesion complexes (ACs). These ACs are dynamic structures that are constantly binding and unbinding. The ECM is simulated as

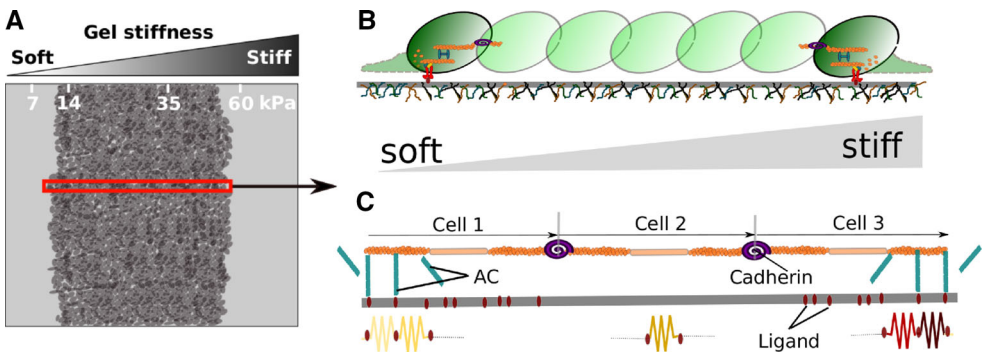

Fig. 1 Cell monolayer model. **a** Schematic of the cell monolayer (dark gray) expanding over a gel with stiffness gradient, based on experiments performed in Sunyer et al. (2016). Model approximation only considers displacements in the direction of the stiffness gradient (red rectangle). **b** The monolayer is composed by several bound cells placed in a substrate with a rigidity gradient. **c** Cells are bound to each other with cadherins. Adhesion complexes (ACs) bind the monolayer with the ligands in the extracellular matrix transmitting the forces and causing the substrate deformation. The ECM, simulated as a set of springs with a variable Young's modulus, presents a stiffness gradient, which guides migration direction and speed

a set of truss elements with a variable stiffness which allows us to reproduce different rigidity gradients. Displacements of the monolayer are considered only in one dimension, along the rigidity gradient direction. The contribution of this model to the literature is considerable since it offers the possibility of simulating both single and collective cell durotaxis. We are able to analyze mechanisms that are crucial to understand how collective behavior emerges and compare it to single cell migration.

That previous work was focused on the experimental findings on how collective behavior emerges from supracellular transmission of contractile physical forces. The model explained the physics behind this phenomenon and was able to reproduce the main experimental results shown there. However, due to the main focus on the experimental findings, the implications and regulation of the proposed model were not explored. Here, we provide an in-depth analysis of the proposed molecular clutch model of collective durotaxis. We incorporate improvements and adjustments to simulate larger time ranges, and we present novel results of the model such as the analysis of the effect of adhesion size or actin velocity. Crucial aspects such as myosin activity, adhesion density, and substrate stiffness sensing are analyzed through a sensitivity analysis. We conclude that collective migration is much more efficient than single cell migration. Force transmission, adhesions size as well as the substrate stiffness difference between adhesive areas are crucial to regulate stiffness-directed migration, and we show qualitative predictions of the emergent behavior in each case.

2 Durotaxis model

We develop a generalized model for simulating single cell or collective cell migration considering the dynamics of cell–matrix adhesions. The model methodology is an expanded version of the one previously presented in Sunyer et al. (2016). These interactions are modeled using a discrete approach based on a local clutch at the corresponding edges of the cell. Fundamental aspects of the mathematical approach are based on previous works that studied cell–ECM adhesion dynamics in filopodia (Escribano et al. 2014). The model consists of three main parts to simulate the dynamics of cell population and to analyze their behavior during migration: the cell monolayer, the ECM, and the adhesion complexes, which are a conglomerate of adaptor proteins that connect the other two parts (Fig. 1). The entire model is composed by truss elements with different properties in order to simulate the different parts. Cell monolayer contains several cells bound to each other by cadherins, which are simulated as springs.

Each individual cell is divided into three different parts (Fig. 2): the first part is a central contractile rod where myosin molecular motors apply forces to contract the actin filaments. The second part consists of two adhesive zones flanking the contractile part, which binds to the ECM through discrete particles called adhesion complexes (ACs). Those represent the different adapter proteins (such as talin, vinculin, paxillin, and integrins) that bind the actin to the ECM (Kanchanawong et al. 2010; Condor and Garcia-Aznar 2017). Finally, there is a protrusive part at each monolayer edge, where the actin monomers polymerize. Due to the high number of elements involved in this kind of process and to the lack of knowledge that there still exists in some of the involved phenomena, some simplifications in the system are necessary when building the model. Thus, this approach simplifies the system by considering only the spatial direction along the stiffness gradient. In the following sections, we describe the mathematical formulation of the model and its corresponding numerical implementation.

The cell monolayer consists of a set of cells, n_{cell}, bound to each other with cadherins. As we have described previously

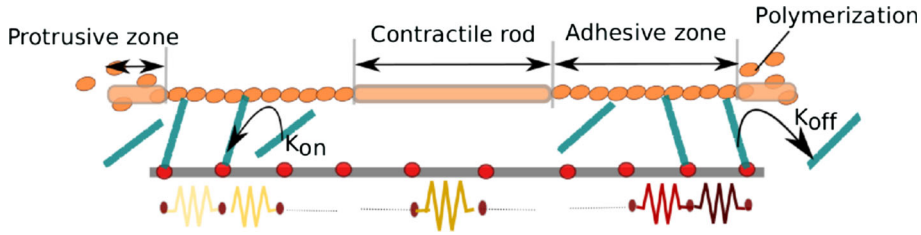

Fig. 2 Schematic of a single cell. Cell (upper horizontal bar) is connected to the substrate (lower black bar) by the adhesion complexes (ACs, blue bars). Contractile forces generated in the cell are transmitted through these ACs to the substrate. The cell consists of a contractile part, an adhesive part, and a protrusive part. The contractile part contracts and pulls the rest of the monolayer. The adhesive part is formed by actin monomers and allows the cell to adhere to the substrate through the ACs. The protrusive part enables the monolayer to expand, adding new actin monomers to the adhesive part

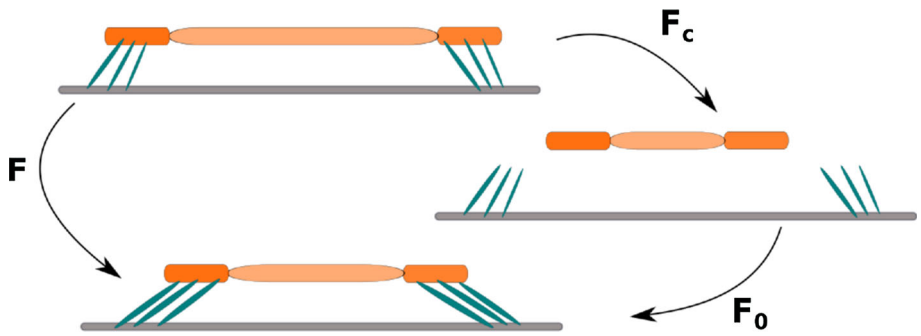

Fig. 3 Explanation of the deformation tensor for contraction. Deformation tensor, $\boldsymbol{F}_{\mathrm{c}}$, is the consequence of myosin activity, and it contracts the central part of the cell (orange). If there is no adhesion to the substrate (gray) or the presence of other cells, no residual stress is generated, and therefore, this deformation is compatible: $\boldsymbol{F}^{\mathrm{cont}} = \boldsymbol{F}_{\mathrm{c}}$. If there are adhesion complexes binding the cell with the ECM, an internal residual stress is generated by these parts and the deformation tensor is not compatible. In this case, an auxiliary compatibility tensor $\boldsymbol{F}_0$ that englobes this internal residual stress is necessary to reach an equilibrium state: $\boldsymbol{F}^{\mathrm{cont}} = \boldsymbol{F}_{\mathrm{o}}^{\mathrm{cont}} \boldsymbol{F}_{\mathrm{c}}$

in Fig. 2, each cell is composed by three main parts. The central contractile part of the monolayer is modeled as a long truss element with variable length on which myosin exerts a constant contraction, pulling on the adhesive and protrusive parts. This contraction is included by means of a gradient deformation tensor, $\boldsymbol{F}_{\mathrm{c}}$. This tensor provokes a contraction in the contractile part which generates no residual internal stress. However, the presence of other cells or the adhesion complexes binding to the substrate might generate residual internal stress which makes $\boldsymbol{F}_{\mathrm{c}}$ incompatible. The total deformation gradient due to contraction $\boldsymbol{F}^{\mathrm{cont}}$ needs to warrant compatibility in the mechanical equilibrium. To make $\boldsymbol{F}^{\mathrm{cont}}$ compatible, an auxiliary tensor $\boldsymbol{F}_{\mathrm{o}}^{\mathrm{cont}}$ is needed. This tensor incorporates the internal residual stress of the system caused by the presence of other cells or adhesions to the substrate Thus, the total deformation is described by the deformation gradient (Rodriguez et al. 1994; Reina-Romo et al. 2010) (see Fig. 3):

$$\boldsymbol{F}^{\mathrm{cont}} = \boldsymbol{F}_{\mathrm{o}}^{\mathrm{cont}} \cdot \boldsymbol{F}_{\mathrm{c}} \tag{1}$$

In general, kinematics of the deformation gradient are expressed (Bonet and Wood 2008) as:

$$F = \frac{\partial \emptyset}{\partial \boldsymbol{X}} \tag{2}$$

where the motion is described by a mapping $\emptyset$ between initial and current particle positions as: $\emptyset = x(\boldsymbol{X}, t)$.

If we consider a small displacement u(x) from the current configuration $\emptyset = x(\boldsymbol{X}, t)$, we can express the displacement gradient tensor $\boldsymbol{L}$ as:

$$\boldsymbol{L} = \frac{\partial u\,(\boldsymbol{x}, t)}{\partial x} \tag{3}$$

where the displacement gradient tensor corresponds to the linearized deformation $\boldsymbol{\varepsilon}$ and rotation tensors $\boldsymbol{w}$:

$$\boldsymbol{L} = \frac{1}{2}\left(\boldsymbol{L} + \boldsymbol{L}^{\mathrm{T}}\right) + \frac{1}{2}\left(\boldsymbol{L} - \boldsymbol{L}^{\mathrm{T}}\right) = \boldsymbol{\varepsilon} + \boldsymbol{w} \tag{4}$$

Deformation gradient tensor can be written in terms of the displacement gradient tensor $\boldsymbol{L}$ using the expression $\boldsymbol{F} = \mathbf{1} + \boldsymbol{L}$, ($\mathbf{1}$ being the unity second-order tensor). Then, if we expand Eq. 1, we obtain:

$$\boldsymbol{F}^{\mathrm{cont}} = \left(\mathbf{1} + \boldsymbol{L}_0^{\mathrm{cont}}\right)(\mathbf{1} + \boldsymbol{L}_{\mathrm{c}}) \tag{5}$$

If we develop this formulation under the small deformation assumption, we have that:

$$\boldsymbol{F}^{\mathrm{cont}} \simeq \mathbf{1} + \boldsymbol{L}_{\mathrm{c}} + \boldsymbol{L}_0^{\mathrm{cont}} \tag{6}$$

Therefore, myosin creates a strain rate on this contractile segment that is regulated by the forces associated to the adhesive complexes, $\boldsymbol{F}_{\mathrm{o}}^{\mathrm{cont}}$. Hence, if there are no ACs connected to the substrate, the contraction from the myosin only occurs in the cell, and it is not transmitted to the substrate, then $\boldsymbol{F}_{\mathrm{o}}^{\mathrm{cont}} = \mathbf{1}$, and the total strain rate of the contractile segment $\boldsymbol{F}^{\mathrm{cont}} = \mathbf{1} + \boldsymbol{L}_{\mathrm{c}}$ is maximum. If there exist ACs connecting the cell to the ECM, the transmitted force increases and opposes contraction, stalling myosin, and cell movement when it reaches $\boldsymbol{F}_{\mathrm{c}}$, and then $\boldsymbol{L}_{\mathrm{c}} = -\boldsymbol{L}_{\mathrm{o}}^{\mathrm{cont}}$, obtaining: $\boldsymbol{F}^{\mathrm{cont}} = \mathbf{1}$.

The adhesive part is composed of a set of actin monomers, each of them allowing the dynamic binding and unbinding of adhesion complexes. This part has a length L_{adhesive} that depends on the initial number of actin monomers, n_{am}, which are separated a distance d_{am}. n_{am} is kept constant throughout the simulation by balancing polymerization and depolymerization at both ends of the adhesive part.

In a similar way, the polymerization part is located at the cell edges in order to simulate the protrusion phenomenon due to actin polymerization and depolymerization. This part is also modeled as a long truss element with variable length, with a constant growth $\boldsymbol{F}_{\mathrm{p}}$, pushing the other cells. Analogously to the contractile part, the total deformation in the polymerization part can be divided into two terms and it is described by:

$$\boldsymbol{F}^{\mathrm{poli}} = \boldsymbol{F}_{o}^{\mathrm{poli}} \cdot \boldsymbol{F}_{\mathrm{p}} \tag{7}$$

Under the small deformations assumption we obtain:

$$\boldsymbol{F}^{\mathrm{poli}} = \mathbf{1} + \boldsymbol{L}_{0}^{\mathrm{poli}} + \boldsymbol{L}_{\mathrm{p}}, \tag{8}$$

where $\boldsymbol{F}^{\mathrm{poli}}$ is the total strain rate of the polymerization part, $\boldsymbol{L}_{\mathrm{p}}$ is the maximal strain rate associated to the cell growth, and $\boldsymbol{L}_{\mathrm{o}}^{\mathrm{poli}}$ is the strain rate due to the resistance that adjacent cells exert on the current cell.

Hence, if there are no surrounding cells and both cell edges are free, there is no constraint strain due to surrounding cells ($\boldsymbol{F}_{\mathrm{o}}^{\mathrm{poli}} = \mathbf{1}$), and the total strain rate of the polymerization segment is maximum and equal to $\boldsymbol{F}^{\mathrm{poli}} = \mathbf{1} + \boldsymbol{L}_{\mathrm{p}}$. However, if there are surrounding cells close to the studied cell, these cells can regulate polymerization growth.

2.1 Particularization to 1D cell monolayer

Although the model is implemented in 2D, the mechanical resolution of the whole system is one-dimensional (1D), considering all the elements as trusses. Here we present the model described previously in the particular case of the 1D approach.

We simulate the myosin retrograde flow applying a constant deformation to the contractile part, $\varepsilon_c(t)$. The displacement gradient tensor is therefore:

$$\boldsymbol{L}_{\mathrm{c}}(t) = \begin{pmatrix} \varepsilon_{\mathrm{c}}(t) & 0 & 0 \\ 0 & 0 & 0 \\ 0 & 0 & 0 \end{pmatrix} \tag{9}$$

$\varepsilon_{\mathrm{c}}(t)$ is related to the maximum velocity of contraction for the unloaded case (that is, without bound ACs) $v_{c,max}$:

$$\varepsilon_{\mathrm{c}}(t) = \frac{L_{\mathrm{cell,c}}(t) - v_{\mathrm{c,max}} \cdot \Delta t}{L_{\mathrm{cell,c}}(t)}, \tag{10}$$

where $L_{\mathrm{cell,c}}(t)$ is the length of the contractile part of the monolayer and Δt is the simulation step time. The elastic modulus of the contractile part, $E_{\mathrm{cell,c}}(t)$, is updated at each time increment to reproduce the known inverse relationship between actin retrograde speed and maximum force exerted by myosin, f_{m} (Chan and Odde 2008).

$$v_{\mathrm{c}}(t) = v_{\mathrm{c,max}} \left(1 - \frac{f_{\mathrm{AC}}(t)}{f_{\mathrm{m}}}\right) \tag{11}$$

where $f_{\mathrm{AC}}(t)$ is the force exerted by the adhesion complexes and $v_{\mathrm{c}}(t)$ is the real contraction velocity for each time step. $f_{\mathrm{AC}}(t)$ is determined by the deformation of the compatibility tensor $\boldsymbol{F}_{\mathrm{o}}^{\mathrm{cont}}$, necessary to obtain the actual deformation of the contractile part that corresponds to the total deformation gradient due to contraction, $\boldsymbol{F}^{\mathrm{cont}}$.

To this end, $E_{\mathrm{cell,c}}(t)$ is updated so that the contraction $\varepsilon_{\mathrm{c}}(t)$ produced by f_{m} results in the maximum myosin contraction speed $v_{c,\mathrm{max}}$ when divided by the duration of each time step of the model, that is:

$$E_{\mathrm{cell,c}}(t) = \frac{f_{\mathrm{m}} \cdot L_{\mathrm{cell,c}}(t)}{\varepsilon_{\mathrm{c}}(t) \cdot A_{\mathrm{cell}} \cdot \Delta t}, \tag{12}$$

where $\mathrm{A}_{\mathrm{cell}}$ is the cell area.

In a similar way, we propose the following formulation for the polymerization. Polymerization only occurs in the protrusive zones provoking their growth and, therefore, the growth of the cell. The maximum polymerization elongation is defined as

$$\boldsymbol{L}_{\mathrm{p}} = \begin{pmatrix} \varepsilon_{\mathrm{p}}(t) & 0 & 0 \\ 0 & 0 & 0 \\ 0 & 0 & 0 \end{pmatrix} \tag{13}$$

with $\varepsilon_{\mathrm{p}}(t)$ related to the maximum polymerization velocity $v_{\mathrm{p,max}}$ (when there are no surrounding cells):

$$\varepsilon_{\mathrm{p}}(t) = \frac{L_{\mathrm{cell,p}}(t) + v_{\mathrm{p,max}} \cdot \Delta t}{L_{\mathrm{cell,p}}(t)} \tag{14}$$

This elongation produces a maximum polymerization force, f_p, exerted over the surrounding cells. In order to conserve a linear relation between f_p and the polymerization velocity, the elastic modulus of this part is also updated at each time step to ensure this relation:

$$E_{\text{cell,p}}(t) = \frac{f_p \cdot L_{\text{cell,p}}(t)}{\varepsilon_p(t) \cdot A_{\text{cell}} \cdot \Delta t} \tag{15}$$

The surrounding cells provoke a deformation corresponding to the compatibility tensor $\boldsymbol{F}_o^{\text{poli}}$. So, the actual deformation of the polymerization part is given by the total deformation gradient due to polymerization $\boldsymbol{F}^{\text{poli}}$.

Therefore, Eq. 14 defines the kinematics associated to the polymerization part of the cell. Hence, after computing $\boldsymbol{F}^{\text{poli}}$ by means of numerical simulations, the length of the contractile part of the cell is updated at each time increment. Depolymerization is also considered by means of updating the length; when the protrusive part length increment is higher than the distance between two actins (d_{am}), a new monomer is added provoking the growth (of d_{am}) of the adhesion zone and the corresponding shrink of the protrusive part. In order to keep the length of the adhesive zone constant at each time that polymerization occurs, depolymerization is forced at the other end of the adhesive zone, which ultimately provokes a growth of d_{am} in the contractile part. In this way, the cell is growing as a consequence of actin polymerization, whereas adhesion zone length is kept constant. The elastic moduli of the contractile and protrusive parts are recalculated at each time step in order to ensure the same linear relation between the contraction or protrusion velocity and the force that opposes to it.

It is important to remark that polymerization is what causes the general cell/monolayer growth. There are no other effects included in the model that causes the growth of the monolayer. In fact, the cell growth is determined by a competition between contraction and polymerization. Both phenomena have been considered independent from each other. Contraction total velocity depends not only on the contraction itself but also on the adhesion with the ECM. Polymerization depends on the actual polymerization velocity and the existence of other cells surrounding the part that is polymerizing.

Finally, we note that the elastic moduli of the different parts of the cell $E_{\text{cell,c}}$, $E_{\text{cell,p}}$, and $E_{\text{cell,a}}$ (contractile, polymerization, and adhesive) merely serve to reproduce a contractile, stiff actin filament and they are not meant to represent actual values of cell stiffness. In fact, the elastic modulus of the contractile and protrusive part varies throughout the simulation in order to ensure the same linear relation (Eqs. 12, 15) between maximum force and maximum contraction independently of the current length of each part.

2.2 Substrate

The substrate is simulated as a set of truss elements with total length L_{sub} and a cross-sectional area A_{sub}. Note that A_{sub} does not coincide with the gel section in experiments since the displacements observed in experiments do not occur through the entire gel substrate depth, but only near the surface. The substrate contains a set of ligand points, which serve as anchoring points for the ACs and are separated a fixed distance, d_{lig}. To model the different stiffness gradient conditions, the stiffness of each truss element E_{sub} (between ligands) is different depending on its spatial location. We assume that the substrate behaves as a linear elastic material where its elastic modulus is defined by E_{sub}.

2.3 Adhesion complexes (ACs)

ACs are modeled as a bar in which one end binds to the actin monomers and the other one to the ligands. Thus ACs can be completely free and moving according to Brownian dynamics, bound only at one edge, or bound at both edges. Force transmission between cells and substrate only occurs in the latter case. Brownian dynamics of free ACs are governed by the Langevin equation (Kim et al. 2007), in which inertial effects are neglected. If we consider the i-th AC,

$$\frac{\mathrm{d}\boldsymbol{r}_i}{\mathrm{d}t} = \frac{1}{\xi}\boldsymbol{F}_i^B \tag{16}$$

where $\boldsymbol{r}_i$ corresponds to the current position of the AC, ξ is the drag coefficient, and $\boldsymbol{F}_i^B$ is a stochastic force. In order to model the Brownian behavior of the adhesion complexes, we consider that these complexes are subjected to stochastic forces approximated as white-noise processes fulfilling the hypothesis of the fluctuation-dissipation theorem (Doyle et al. 1997), that is, they must satisfy the following relations:

$$\begin{aligned} \langle \boldsymbol{F}_i^B(t) \rangle &= 0 \\ \langle \boldsymbol{F}_i^B(t) \boldsymbol{F}_j^B(t) \rangle &= 2k_{\text{B}} T \xi_i \delta_{ij} \delta(t - t'), \end{aligned} \tag{17}$$

where k_{B} is the Boltzmann constant, T the absolute temperature, ξ_i the drag coefficient, δ_{ij} the Kronecker delta, and δ the Dirac delta function (it means that when $t \simeq t'$, then $\delta \to \infty$). In order to simulate these forces numerically, an equivalent discrete form of the previous equations during an individual time step, beginning at time t and ending at time $t + \Delta t$, is considered:

$$\begin{aligned} \langle \boldsymbol{F}_i^B(t) \rangle &= 0 \\ \langle \boldsymbol{F}_i^B(t) \boldsymbol{F}_j^B(t) \rangle &= \frac{2k_B T \xi_i \delta_{ij}}{\Delta t} \boldsymbol{\delta}, \end{aligned} \tag{18}$$

where k_{B} is the Boltzmann constant, T the absolute temperature, $\boldsymbol{\delta}$ the second-order unit tensor, and Δt the time

increment considered in the simulation. We considered for simplicity that the geometry of the AC corresponds to a sphere with drag coefficient $\xi_i = 6\pi\eta r_{\mathrm{AC}}$, being r_{AC} the radius of the sphere and η the viscosity of the medium (Escribano et al. 2015).

Binding and unbinding of ACs to the actin filaments and to the substrate are modeled through binding rates k_{bind} and unbinding rates $k_{\mathrm{ub}}^{\mathrm{cb}}$. Binding rates are modeled according to the Bell equation as a function of the distance between them:

$$k_{\mathrm{bind}} = k_{\mathrm{bind}}^{0}\exp\left(-\lambda_{\mathrm{bind}} \cdot d_{\mathrm{b}}\right), \tag{19}$$

where λ_{bind} is the mechanical compliance for creating the bond, k_{bind}^{0} is the zero-distance binding coefficient, and d_{b} is the distance between the adhesion complex and the closest ligand or actin binding site.

Unbinding is modeled as a catch/slip bond law, experimentally proved in different integrins (Novikova and Storm 2013):

$$k_{\mathrm{ub}}^{\mathrm{cb}} = \exp\left(\emptyset_{\mathrm{c}} - \emptyset\right) + \exp\left(\emptyset - \emptyset_{\mathrm{s}}\right), \tag{20}$$

with $\emptyset = F_b/F^*$, where $\emptyset_c, \emptyset_s$ are the parameters of the catch and slip bond regimes, respectively, F^* is used to normalize the force, and F_b is the modulus of the current force for the specific adhesion complex (modulus of the local force transmitted from the cell to the substrate).

2.4 Model implementation

Computational simulations are implemented using the finite element method (FEM), under the assumption of small deformations and considering that all the mechanical components present a linear elastic behavior. Nevertheless, a dissipative analysis is required due to the friction between the cell monolayer and the surrounding medium. All equations are implemented in a C++ code developed by the authors. Simulations start with all the ACs unbound and free, and the monolayer expanding symmetrically at both edges in such a way that the speed of actin polymerization dominates over contraction. Figure 4 shows the algorithm that is carried out after initialization at each time step increment. The parameters used in the model are given in Table 1.

We have made a 1D approximation of a 3D problem where we analyze the system in one direction (the one along the gradient). Since we assume that this direction is much longer than the other two, we can simulate all the elements as a set of rods with a given length, area, and Young's modulus. The behavior of the system can be expressed in terms of the global stiffness matrix, **K** (Hughes 1987). The displacement field $\boldsymbol{d}$ at the cell monolayer and the substrate are computed through the finite element method, considering both elastic forces and a friction coefficient between the cell monolayer

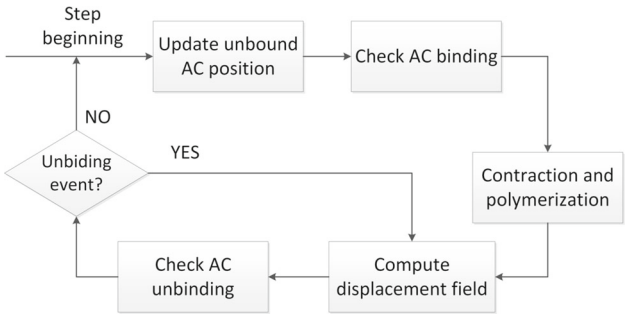

Fig. 4 Computational algorithm for each time step. First we calculate unbound AC locations through Langevin equation and then check whether a binding event occurs. Binding depends on AC distance to ligand or actin monomer. After we apply cell contraction and actin polymerization and compute the resulting displacement field, then, from the displacement field we calculate bound AC forces to determine whether they unbind or not. If any unbinding event occurs, we recalculate the displacement field and this process is repeated until no unbinding occurs and the system is in equilibrium

and the surrounding medium, that is:

$$\boldsymbol{C}\dot{\boldsymbol{d}} + \boldsymbol{k}\boldsymbol{d} = \boldsymbol{F}, \tag{21}$$

where $\boldsymbol{C}$ is the viscous damping matrix only associated to the cell monolayer (adhesive and protrusive parts) and $\boldsymbol{F}$ is the external global force vector. For this particular model, external global forces are zero ($\boldsymbol{F} = 0$) since cell contraction and polymerization are included as a deformation of the bar, and therefore, they are considered as internal forces.

The global stiffness matrix $\boldsymbol{K}$ is built from the assembly of the local stiffness matrix at each element i:

$$\boldsymbol{K}^i = \begin{pmatrix} \frac{E^i A^i}{L^i} & \frac{-E^i A^i}{L^i} \\ \frac{-E^i A^i}{L^i} & \frac{E^i A^i}{L^i} \end{pmatrix}, \tag{22}$$

where E^i is the elastic modulus of the element i (belonging either to the cell, the substrate, or the adhesion complex), and A^i and L^i are the area of the rod section and length of the rod, respectively (Hughes 1987).

A particular convenient form of the viscous damping matrix associated to the degrees of freedom of the cell monolayer (in the adhesive and protrusive parts) is the Rayleigh damping matrix:

$$\boldsymbol{C}^i = \frac{\varsigma}{\rho}\boldsymbol{M}^i = \frac{1}{2}\varsigma L^i \begin{pmatrix} 1 & 0 \\ 0 & 1 \end{pmatrix} \tag{23}$$

where ς is the friction coefficient associated to the surrounding medium (this coefficient is fixed to be Kg/nm.s to assure adequate units of $\mathbf{C}^{\mathrm{i}}$ as Kg/s.), ρ is the density of the cell monolayer, and $\boldsymbol{M}^i$ is the diagonal mass matrix associated to the cell monolayer.

Table 1 Model parameters

Parameter	Symbol	Value
Boltzmann energy	$k_B T$	4.142×10^{-21} (J)
Myosin force	f_m	630 (pN)
Unloaded contraction velocity	$v_{c,max}$	80 (nm/s)
Polymerization force	f_p	15 (pN)
Maximum polymerization velocity	$v_{p,max}$	12 (nm/s)
AC radius	r_{AC}	40 (nm)
Force to normalize parameters in catch bond law	F^*	3 (pN)
Nondimensionalized force of catch curve in catch bond law	$\emptyset_c$	0.6025
Nondimensionalized force of slip curve in catch bond law	$\emptyset_s$	10.2112
Medium viscosity for the AC arm	η	8.59×10^{-4} (Pa s)
Friction between cell and the surrounding medium	ς	3.5×10^4 (Pa s)
Mechanical compliance of the AC for creating the bond	λ_{bind}	0.1 (nN^{-1})
Zero-force binding coefficient	k^0_{bind}	100 (s^{-1})
Cell adhesive part elastic modulus	$E_{cell,a}$	5×10^7 (Pa)
Monolayer total length	L_{cell}	5×10^5 (nm)
Cell area	A_{cell}	8×10^5 (nm^2)
Cell adhesive part length	$L_{adhesive}$	6×10^3 (nm)
Distance between actin monomers	d_{am}	25 (nm)
AC spring constant	K_{AC}	0.1N/m
Substrate length	L_{sub}	2.5×10^6 (nm)
Substrate area	A_{sub}	2.2×10^7 (nm^2)
Distance between ligands	d_{lig}	100 nm
Simulation step time	Δt	0.03 s
Total time of the simulation	T	360 s

These parameters could be found in the literature, and their values are maintained within a range. Myosin force and unloaded contraction velocity have been selected within the ranges observed in previous works (Elosegui-Artola et al. 2014, 2016). Parameters of the catch bond law are according to average lifetime reported for FN − α 5 β 1 (Kong et al. 2009). Actin polymerization velocities are obtained from values reported for actin flow after myosin inhibition (Gardel et al. 2008). Binding properties have been selected in order to ensure a strong adhesion which allows a better force transmission; values are within the range used in (Elosegui-Artola et al. 2014). Size of the adhesion complexes is within the range of experimental observations of focal adhesion architecture (Kanchanawong et al. 2010). Polymerization velocity is set, so total growth of the monolayer correlates with experimental observation (Sunyer et al. 2016). Polymerization force is set within values reported in (Ananthakrishnan and Ehrlicher 2007)

Due to the time dependence of the model, in order to solve the mechanical problem at each time step, we use a backward Euler method, that is:

$$\boldsymbol{C}\boldsymbol{v}_{n+1} + \boldsymbol{K}d_{n+1} = \boldsymbol{F}_{n+1} \tag{24}$$

$$\boldsymbol{v}_{n+1} = \frac{\boldsymbol{d}_{n+1} - \boldsymbol{d}_n}{\Delta t} \tag{25}$$

where d_{n+1} and F_{n+1} are the temporal approximations of $\boldsymbol{d}(t_{n+1})$ and $\boldsymbol{F}(t_{n+1})$, respectively. In particular, we have implemented the d-form proposed by Hughes (2012):

$$\frac{1}{\Delta t}\left(\boldsymbol{C} + \Delta t \boldsymbol{K}\right)\boldsymbol{d}_{n+1} = \boldsymbol{F}_{n+1} + \frac{1}{\Delta t}\boldsymbol{C}\boldsymbol{d}_n. \tag{26}$$

3 Results

We aim to test the ability of the model to predict the durotaxis event under different conditions according to experimental measurements. We use different types of substrates with different stiffness gradients: steep gel, shallow gel, and uniform gel (constant rigidity). Steep gel possesses a higher gradient than the shallow gel (Fig S1). We simulate a cell monolayer for a specific length placed in different initial position on the substrate (different initial stiffness) for each of the gradients. We refer to this initial position as stiffness offset. The only parameter tuned for the different conditions is the elasticity modulus of the substrate, in order to reproduce the corresponding stiffness gradient and the initial monolayer stiffness offset, that have been used in the experiments.

Durotaxis in the model is caused by two different processes. The first one is the mechanical balance between the forces transmitted through the adhesions at both ends of the cells. Force balance causes the deformation of the substrate, which is higher in the softer part than in the stiffer part. This generates a directional movement toward the stiffer part (see Fig S2 and video S3). The second one is cell growth. Two mechanisms affect cell growth: the actin retrograde flow that is originated by myosin activity and provokes the cell shrinking, and actin polymerization, which causes cell growth. Balance between these two effects results in the effective cell growth velocity.

We test our model under different conditions. First, we establish two behavior hypotheses in order to understand the difference between single and collective cell migration and observe how different stiffness offsets in the gel along the stiffness gradient influence the effectiveness of the directional movement. Moreover, we compare our numerical results with experimental data. Then, we study different aspects on both edges of the monolayer (low and high stiffness) for different offsets and different gels: their movement and the actin retrograde velocity. Finally, we perform a sensitivity analysis identifying different parameters that are relevant to the durotaxis processes.

Results shown in this work are based on experimental results obtained by the same authors in Sunyer et al. (2016). Here, we use the same stiffness gradients and similar stiffness offsets in order to validate the model output with the experiments. The validation of the results is carried out in terms of velocity. In order to compare displacement results

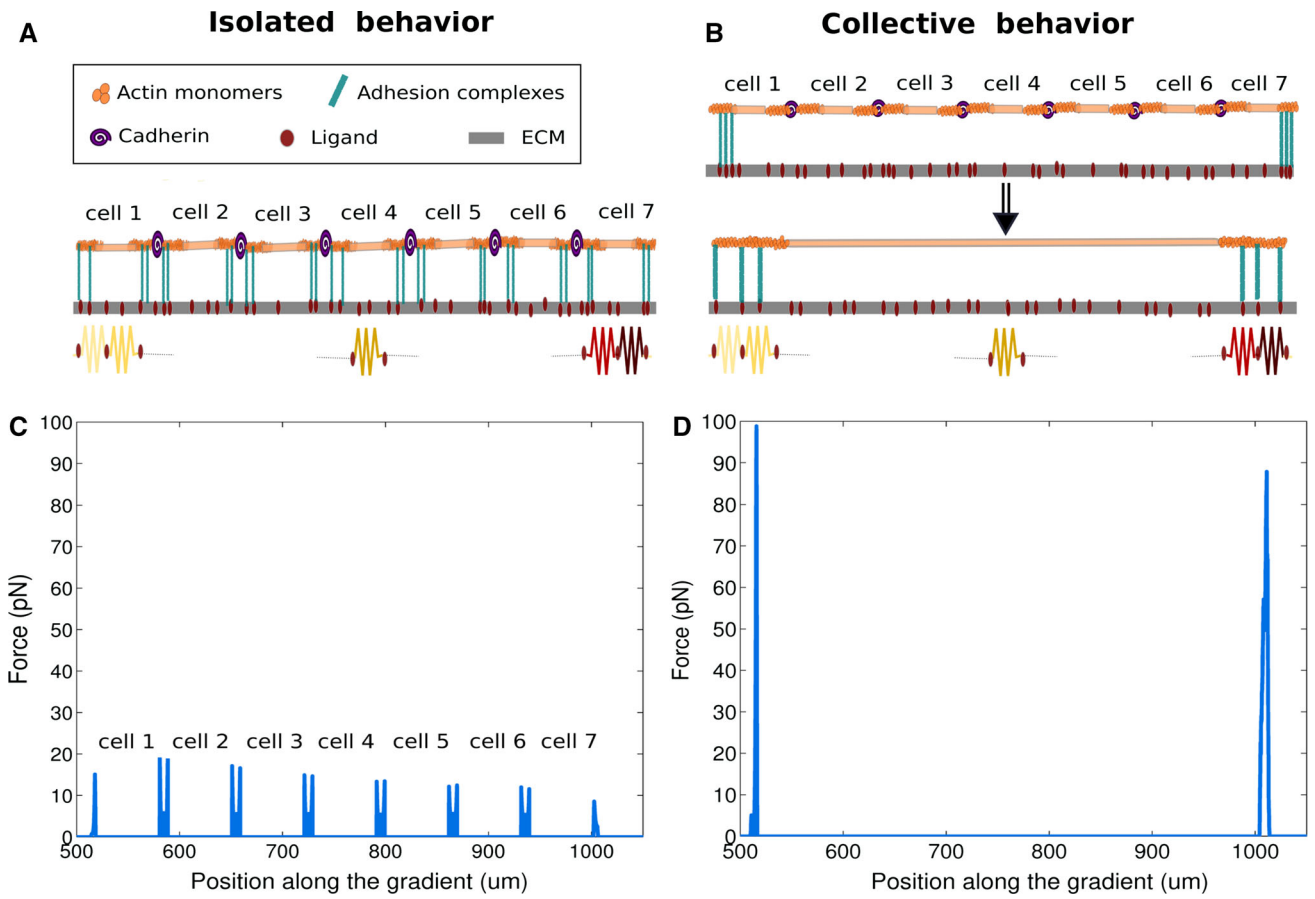

Fig. 5 Isolated versus collective cell behavior. Comparison between both hypotheses proposed for cell movement. Cell (orange) contraction forces, originated by myosin activity, are transmitted to the substrate by the adhesion complexes. These adhesion complexes adhere to the actin monomers in the cell and to the ligands in the ECM. The ECM is composed by a set of springs in series. Each spring has different stiffness in order to simulate the rigidity gradient. In isolated behavior each cell behaves in an independent way. Each of them adheres to the substrate transmitting the force. In collective behavior, cells inside the monolayer are driven by the cells in the border. Adhesion and therefore force are concentrated at the monolayer edges. (**a**) and (**b**). Schematic for each type of behavior. For collective behavior (**b**), since adhesion only occurs at both ends, the monolayer is simulated as a long single cell for simplicity. **c** Simulation results of force exerted by the monolayer over the substrate for isolated behavior at the final time step (monolayer composed by 7 cells). **d** Simulation results of force exerted by the monolayer over the substrate for collective behavior at the final time step

with experimental data, simulations are linearly extrapolated from 6 minutes to 10 hours to accelerate calculation time due to the great number of different offsets. Simulating ten hours is computationally expensive, and the results do not change significantly (Fig S4).

3.1 Collective cell durotaxis is more efficient than isolated cell durotaxis

First, we compare isolated and collective behavior (Fig. 5). In isolated behavior, each individual cell contracts and adheres to the ECM on both sides. Each cell behaves as if it is isolated, without showing any kind of collective behavior. Our simulations show that cells inside the monolayer exert peak forces over the ECM, Fig. 5c. However, it has been observed experimentally (Tambe et al. 2011; Sunyer et al. 2016) that higher forces are more likely to concentrate in both ends of the monolayer than in the middle of it. This suggests the existence of a mechanism that regulates collective behavior where cells in the middle are driven by the cells on the monolayer border. Based on these observations, we make the assumption that only cells in the monolayer edges adhere to the substrate and that forces inside the monolayer are fully transmitted through cell–cell adhesion from one edge to edge. In order to simulate this collective cell behavior, for simplicity, we assume the monolayer as a long cell that only adheres at its border (Fig. 5b). We can observe that for this case, forces concentrate on the monolayer borders (Fig. 5d).

With the aim of testing the efficiency of both mechanisms in exhibiting durotaxis, we run a test where we place different monolayers in different initial stiffness offsets and we track the movement of the monolayer center (Fig. 6). Simulations

for both hypotheses are compared with experimental data (Sunyer et al. 2016). Tests are done for two different rigidity gradients (steep gel and shallow gel) and a case with constant rigidity (uniform gel). Cell monolayers with isolated behavior exhibit considerably lower durotaxis than experimental results and barely show sensitivity to the stiffness offset. These results for isolated behavior also correlate with experimental observations where cell connections were altered by the depletion of α-catenin in order to avoid collective behavior (Sunyer et al. 2016). Force transmission between cells and ECM inside the monolayer critically reduces their ability to sense the stiffness gradient and provokes a reduction on the directional movement toward the stiffer part. Results for collective behavior assumption, where force accumulates at the borders of the monolayer, show a considerable higher ability to follow the stiffness gradient and more sensitivity to changes in the stiffness offset. In general, durotaxis is higher when the monolayer is initially placed in the softer substrate position. The ability of cells to migrate with directionality is coupled with the rigidity gradient that they are able to sense. This is determined by the difference in the substrate stiffness between both sides where the cell monolayer is attached. When the cell monolayer is placed in the softer part of the gradient, the stiffness difference between both sides is higher than when it is placed in the stiffer part due to the exponential nature of the stiffness gradient. For gels without rigidity gradient (Fig. 6c) directional movement is lost, and the monolayer grows symmetrically toward both sides.

3.2 Stiffer edge of the cell monolayer advances faster than the softer one

If we analyze both edges of the monolayer (Fig. 7) we observe that the edge located in the stiffer part grows faster than the one located in the softer one. The growth of each part depends on the stiffness of the substrate where it is located. If we observe actin retrograde velocity of each side of the monolayer (Fig. 8) we find that in the stiffer part retraction velocity is lower than in the softer part for both steep and shallow gels. This is consistent with previous experiments, where this same effect was described (Sunyer et al. 2016).

A constant polymerization velocity with a lower retraction velocity means a higher growth. This higher growth of the stiffer part, coupled with the movement toward the stiffer part of the monolayer due to the force balance and the higher deformability of the softer part, provokes the higher growth in the stiffer part of the cell monolayer observed in the simulations (see video S5).

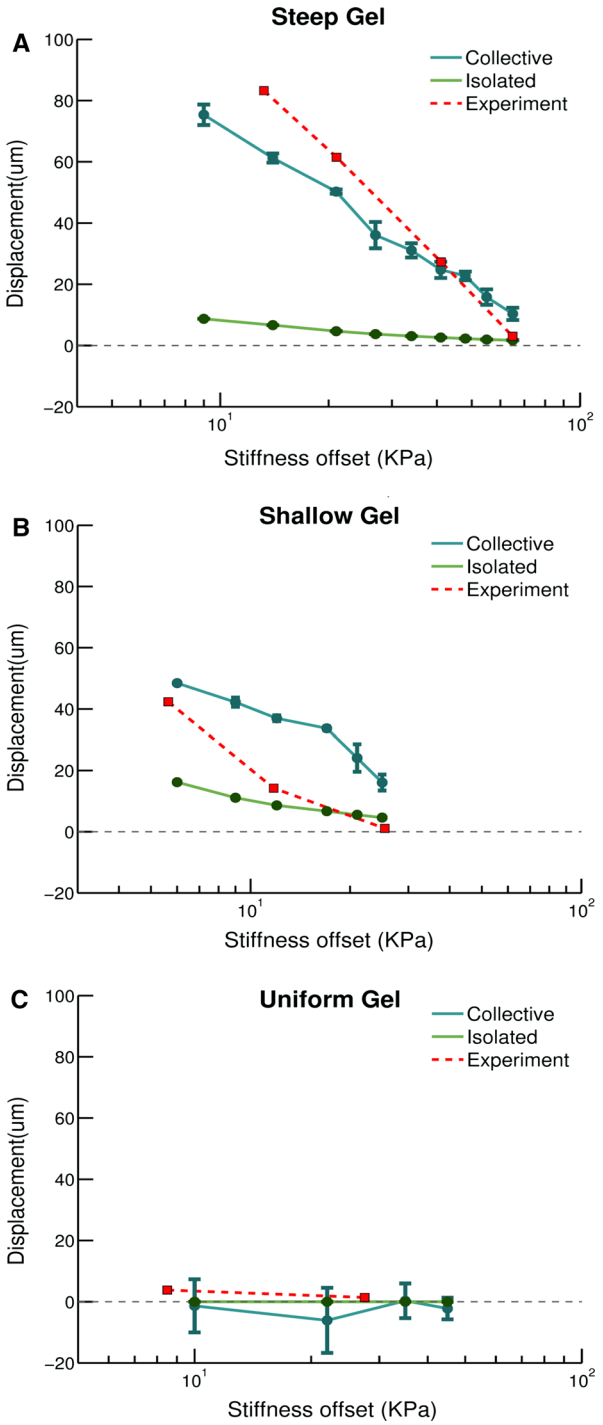

Fig. 6 Isolated versus collective durotaxis. Movement of the center of mass of different monolayers after 10 h. Cell monolayers are placed in different initial positions of the substrate (stiffness offset). The horizontal axis represents the initial rigidity at which the monolayer center is placed in the substrate rigidity gradient. Color represents the two different hypotheses of behavior: isolated behavior (green) and collective behavior (blue). Red color corresponds to experimental measurements from Sunyer et al. (2016). Numerical results correspond to the mean of a sample with a population $n = 10$. Error bars are the standard deviation. **a** Movement of the center of mass with a steep gel. **b** Movement of the center of mass with a shallow gel. **c** Movement of the center of mass in a uniform gel (without rigidity gradient)

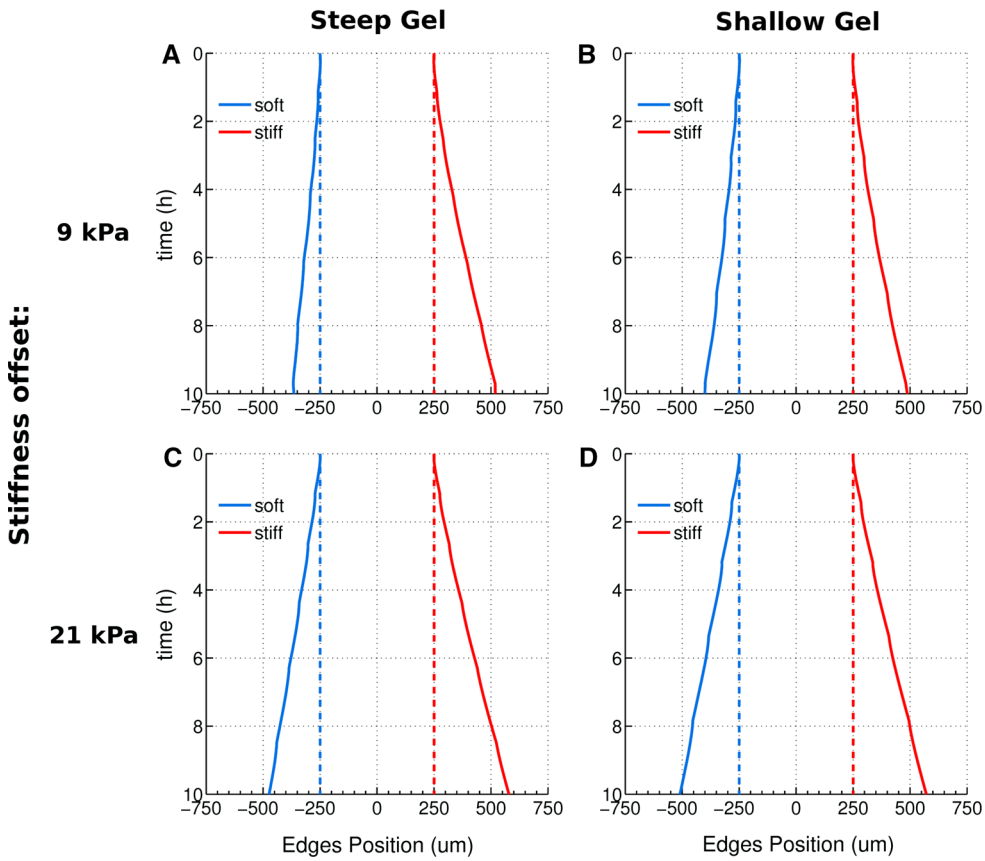

Fig. 7 Cell monolayer edges growth. Position of both edges of the cell monolayer (horizontal axes) during the simulation time (vertical axes). Left column corresponds to steep gel and right column to shallow gel. **a**, **b** Stiffness offset of 9 kPa. **c**, **d** Stiffness offset of 21 kPa

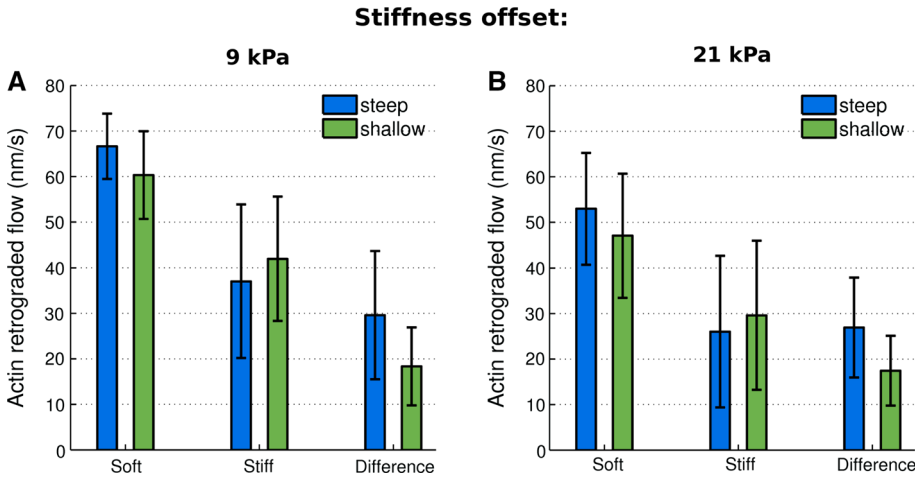

Fig. 8 Actin retrograde velocity comparison between both cell monolayer edges. Actin retrograde velocity average of one simulation case for the two different rigidity gradients. Velocity difference between stiff and soft edge is shown. Error bars correspond to the standard deviation. **a** Results for a 21-kPa stiffness offset. **b** Results for a 9-kPa stiffness

3.3 Larger monolayers are more sensitive to stiffness gradients

In order to test the ability of cells to migrate with stiffness directionality depending on the rigidity gradient that they are able to sense, we change the monolayer length (Fig. 9a, b) for steep and shallow gels, respectively. We observe that a variation in the length results in a variation of the rigidity gradient that the cell monolayer is able to sense, and it influences the ability of cells to move toward the stiffer part of the substrate. Increasing the monolayer length, and therefore the rigidity difference between both adhesive parts, increases directional migration.

This correlates with experimental observations (Sunyer et al. 2016), and it also explains the mechanism by which collective migration is more effective than single cell migration. In our simulations, single cell would correspond to a monolayer of the size of a cell, which will show much less sensitivity to the gel gradient.

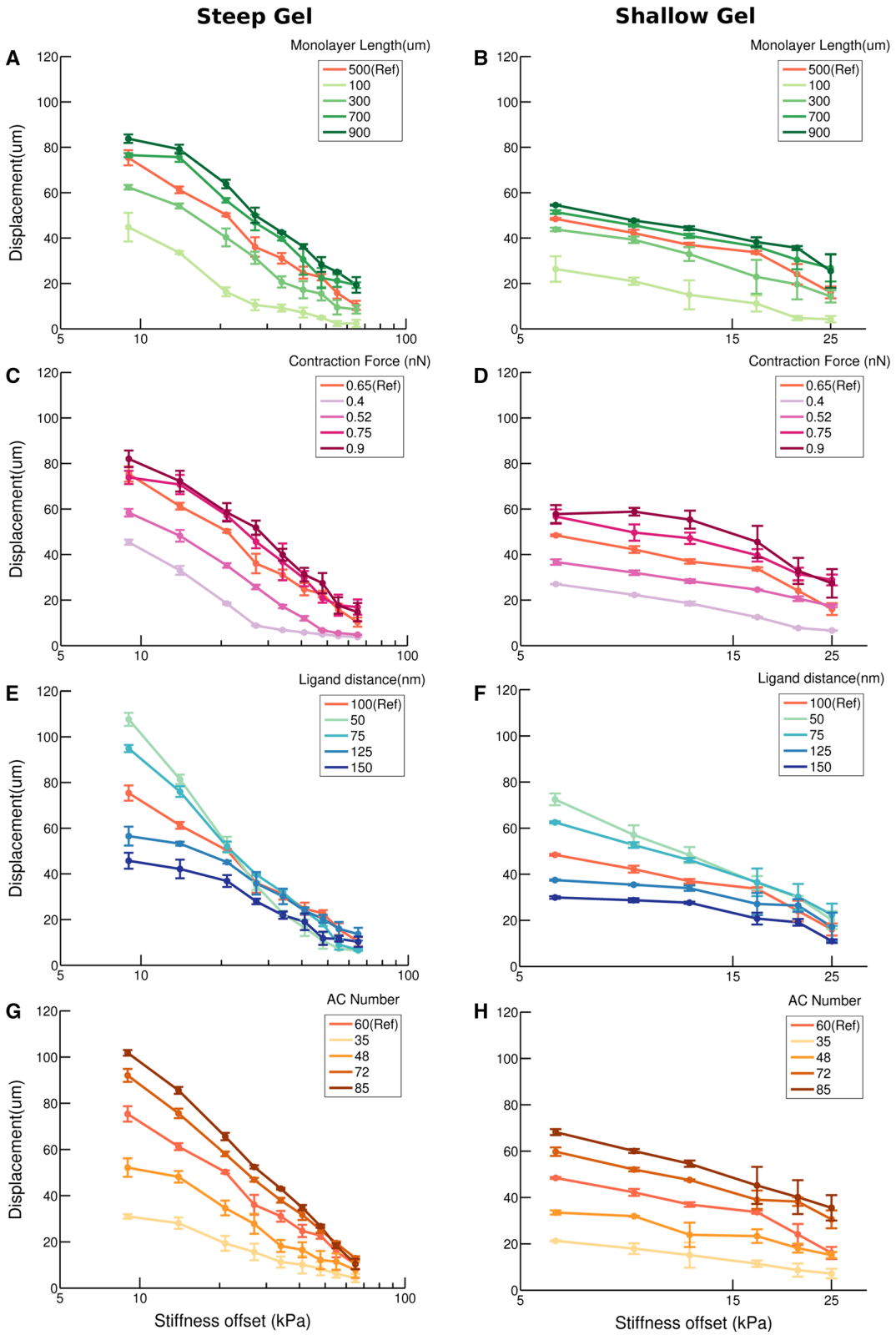

Fig. 9 Sensitivity analysis. Displacement of the cell monolayer center for different stiffness offset. Key parameters are changed, and results are compared to the reference case. The first column corresponds to a steep gel and second column to a shallow gel. Results are the average of $n=5$ simulations, and error bars correspond to standard deviation. **a**, **b** Variation in the monolayer length. **c**, **d** Change in the contraction force of the monolayer. **e**, **f** Variation in the number of adhesion complexes available in each adhesion zone. **g**, **h** Ligand density, tuned by modifying the separation between the ligands in the substrate

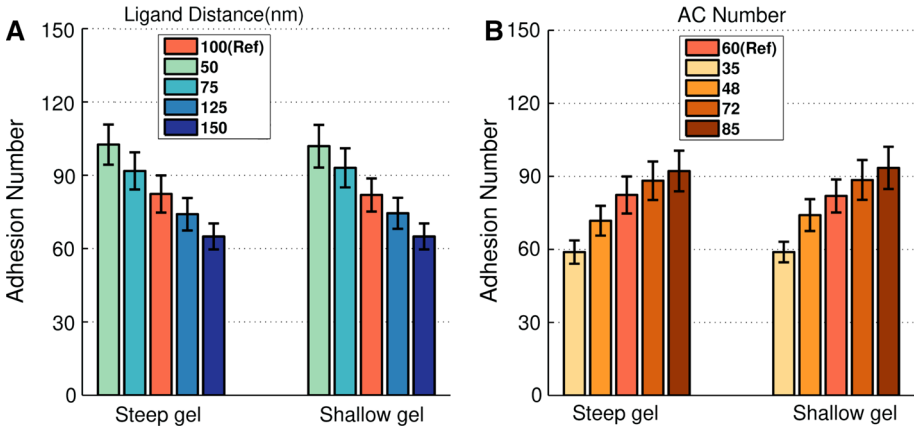

Fig. 10 Cell–ECM discrete adhesion number. Average number of adhesions (bound adhesion complexes) during the total simulation time. Simulations correspond to an offset of 9 kPa for both steep and shallow gel. **a** Variation in the number of adhesion complexes available in each adhesion zone. **b** Varying distance between the ligands in the substrate

3.4 Myosin contractility promotes durotaxis

Cells are able to sense the rigidity gradient by means of force transmission from the cytoskeleton to the substrate through adhesion proteins. Therefore, we expect to obtain a reduction in the gradient sensitivity by means of decreasing this force transmission. To this end, we study the role of cell contraction on the cell monolayer migration. Figure 9c and d shows that a reduction in myosin contractile force also reduces durotaxis. This effect correlates with experimental observations (Sunyer et al. 2016), where blebbistatin added to reduce myosin contractility provoked monolayers to grow more uniformly at both edges, therefore exhibiting less durotaxis.

3.5 Adhesion is crucial to regulate durotaxis

Cell–matrix adhesion has a relevant impact on force transmission. Therefore, we expect to obtain a significant impact on directional migration when we modify adhesion characteristics. We simulate this effect by changing AC density at each side of the monolayer. In Fig. 9e and f we observe that a reduction in adhesion also reduces the ability of the monolayer to sense the stiffness gradient, provoking a more uniform growth at both edges which ultimately results in less durotaxis.

A different way of tuning adhesion in the model is to change the ligand density in the substrate. This could be done by reducing or increasing the distance between them. Results are shown in Fig. 9g and h where the same effect as the one observed with the change in AC density is obtained.

Figure 10 shows how the average number of discrete adhesions for different cases confirms that the number of adhesions is indeed responsible for the observed behavior.

4 Discussion

We have proposed a computational approach that explains the well-known low to high stiffness motion in substrates with rigidity gradients as an emergent phenomenon caused by the force balance between cell–ECM adhesions. In our model, durotaxis occurs due to the ability of cells to deform the substrate more in the part of lower stiffness than in the stiffer part. Then, force balance results in preferential directional movement toward the stiffer part. Previous interesting approaches for modeling durotaxis (Novikova et al. 2017) explained this phenomenon for single cells as a persistence-driven process. The persistence time of cell motion was dependent on substrate rigidity, and based on experimental observations, it was set higher for stiffer substrates. Our physical approach offers a different way of explaining durotaxis, although it is complementary to this previous explanation. In fact, we could observe how higher persistence movement for stiffer substrates emerges from our simulations (Fig S6). It is also worth to mention some other works where negative durotaxis was reported (Singh et al. 2014; Bookholt et al. 2016; Hartman et al. 2016). The fundamental physics of the durotaxis phenomenon presented in this work is not contrary to what it was observed in these other previous works. In fact, migration is the result of the competition between different mechanisms, not only durotaxis as we have considered in this work. If cues due to durotaxis are not as strong as others, like chemotaxis, durotaxis is not going to be the main mechanism that regulates migration. This might result in migration toward softer parts of the matrix depending on these other potential mechanisms activated by other stimuli (Del Amo et al. 2017). Actually, even in the absence of other different factors regulating migration, in single cells or very shallow stiffness gradients cases, the mechanotransduction mechanism proposed here might not be strong enough to regulate migration. In such cases migration could be regulated by other force-sensing mechanism like sub-micrometer contractions that occur in a few seconds at the cell borders during the formation of nascent integrin adhesions (Wolfenson et al. 2016).

Model is designed to reproduce experiments of 2D migration, and it could also be valid for 3D migration. However, we

have to keep in mind that although the physics that regulate our model are still valid in 3D migration, their contribution to the overall competition between the different mechanisms that regulates migration is going to be much less effective than in 2D migration. In 3D migration there are additional effects regulating migration that are not present or have less impact in 2D migration, such as pore size, porosity, permeability, and matrix degradation. In fact, 3D migration is impaired by steric hindrance (Lang et al. 2015; Del Amo et al. 2017; Movilla et al. 2017)

The model presented here allows us to compare single motility with collective cell migration and to understand the underlying mechanisms that make collective migration much more efficient than single cell migration. For this matter, we consider two main types of behavior for cell monolayers: collective or isolated. In isolated behavior all cells contract and adhere to the substrate as individual entities. As a consequence of this individual connection to the substrate, transmission of forces between cell–cell connections is not effective, impeding cell monolayer from sensing the gradient. All of this results in much less efficiency in durotaxis. This is in line with previous experimental results where cell–cell junctions were inhibited (Sunyer et al. 2016) and directional movement toward the stiffer part was critically reduced. For collective behavior, based on experimental observations (Tambe et al. 2011; Sunyer et al. 2016), we assume that forces exerted over the substrate accumulate at both edges of the monolayer. Cells inside the monolayer do not adhere to the substrate and are driven by the cells in the border. This provokes a more efficient transmission of forces through the monolayer, enabling a better stiffness gradient sensing which ultimately results in higher durotaxis. In order to simulate this behavior, for simplicity, we simulate all the monolayer as a long single cell that only adheres to the monolayer at their edges. The reason for this is that if passive cells inside the monolayer do not adhere to the substrate, then their contraction and polymerization in the model are formally equivalent to simply considering one big cell. For this case durotaxis is clearly observed.

Results are also in concordance with other previous works that showed that collective movement is more efficient than isolated cell movement (Merkher and Weihs 2017). Moreover, results in both behavior hypotheses (isolated and collective) correlate with experimental data of our previous work (Sunyer et al. 2016), showing the same trend and adjusting with relative accuracy. We do not only validate results in terms of final displacement of the monolayer, but we also observe how actin velocities and monolayer growth emergent behavior correlate with experimental measurements.

A sensitivity analysis shows interesting evidence on how durotaxis can be regulated by different mechanisms. Cell monolayer size regulates gradient sensing. Single cells sense a smaller range of the stiffness gradient than a cell monolayer. This difference increases as the monolayer becomes bigger. Force transmission from the cell to the substrate is also observed to play a major role in gradient sensing. By reducing myosin contractility, we also obtain a decrement in durotaxis. The same effect is reported when reducing the overall localized number of cell–substrate adhesions. In fact, substrate adhesions have been reported as a crucial factor in other works on durotaxis (Plotnikov et al. 2012; Yu et al. 2017). Adhesion is known to be higher in the stiffer part than in the softer part. In our work, adhesion properties are only modeled in terms of a catch-slip bond law, with no specific relation to stiffness. If we compare adhesion in different rigidities (Fig S7), we observe that in the stiffer parts adhesion is slightly higher, although difference is not significant. Promoting this adhesion difference in terms of rigidity seems a complementary way of promoting durotaxis.

There are some aspects that have not been considered here and could also play an important role in durotaxis, for example, cell proliferation in the monolayer, adhesion spatial distribution on a 2D plane, or the previously mentioned more significant difference between overall adhesion number in softer parts of the gel than in stiffer parts of the gel which could be modeled as the well-known adhesion reinforcement that occurs under higher force rates (Elosegui-Artola et al. 2014). However, in summary, our model presents an intuitive approach to simulate durotaxis as the consequence of the cell's ability to deform the substrate more in its softer part than in the stiffer one. This explanation is compatible and consistent with other models proposed in the literature (Novikova et al. 2017). The possibility of simulating not only single cells but also collective migration under stiffness gradients adds a significant advance to the existing literature.

Acknowledgements This work is supported by the Spanish Ministry of Economy and Competitiveness/FEDER (FPI BES-2013- 063684 to J.E., DPI201564221C21R to J.M.G.-A., BFU2016-79916-P and BFU2014-52586-REDT to PR-C, BFU2015-65074-P to XT), the Generalitat de Catalunya (2014-SGR-927 to XT and CERCA program), the European Research Council (StG 306571 to J.M.G.-A. and CoG-616480 to XT), European Commission (Grant Agreement SEP-210342844 to PR-C and XT). IBEC is recipient of a Severo Ochoa Award of Excellence from the MINECO.

References

Allena R, Scianna M, Preziosi L (2016) A Cellular Potts model of single cell migration in presence of durotaxis. Math Biosci 275:57–70. https://doi.org/10.1016/j.mbs.2016.02.011

Aman A, Piotrowski T (2010) Cell migration during morphogenesis. Dev Biol 341:20–33. https://doi.org/10.1016/j.ydbio.2009.11.014

Ananthakrishnan R, Ehrlicher A (2007) The forces behind cell movement. Int J Biol Sci 3:303–317. https://doi.org/10.7150/ijbs.3.303

Bonet J, Wood RD (2008) Nonlinear continuum mechanics for finite element analysis. Cambridge University Press, Cambridge

Bookholt FD, Monsuur HN, Gibbs S, Vermolen FJ (2016) Mathematical modelling of angiogenesis using continuous cell-based models.

Biomech Model Mechanobiol 15:1577–1600. https://doi.org/10.1007/s10237-016-0784-3
Boon WM, Koppenol DC, Vermolen FJ (2016) A multi-agent cell-based model for wound contraction. J Biomech 49:1388–1401. https://doi.org/10.1016/j.jbiomech.2015.11.058
Camley B, Rappel W-J (2017) Physical models of collective cell motility: from cell to tissue. J Phys D Appl Phys 50:113002. https://doi.org/10.1088/1361-6463/aa56fe
Camley BA, Zhang Y, Zhao Y et al (2014) Polarity mechanisms such as contact inhibition of locomotion regulate persistent rotational motion of mammalian cells on micropatterns. Proc Natl Acad Sci 111:14770–14775. https://doi.org/10.1073/pnas.1414498111
Chan CE, Odde DJ (2008) Traction dynamics of filopodia on compliant substrates. Science 322:1687–1691
Chen J, Weihs D, Vermolen FJ (2017) A model for cell migration in non-isotropic fibrin networks with an application to pancreatic tumor islets. Biomech Model Mechanobiol. https://doi.org/10.1007/s10237-017-0966-7
Cherry JL, Adler FR (2000) How to make a biological switch. J Theor Biol 203:117–133. https://doi.org/10.1006/jtbi.2000.1068
Cochet-Escartin O, Ranft J, Silberzan P, Marcq P (2014) Border forces and friction control epithelial closure dynamics. Biophys J 106:65–73. https://doi.org/10.1016/j.bpj.2013.11.015
Collins JJ, Gardner TS, Cantor CR (2000) Construction of a genetic toggle switch in Escherichia coli. Nature 403:339–342. https://doi.org/10.1038/35002131
Condor M, Garcia-Aznar JM (2017) A phenomenological cohesive model for the macroscopic simulation of cell-matrix adhesions. Biomech Model Mechanobiol. https://doi.org/10.1007/s10237-017-0883-9
Del Amo C, Borau C, Movilla N et al (2017) Quantifying 3D chemotaxis in microfluidic-based chips with step gradients of collagen hydrogel concentrations. Integr Biol 9:339–349. https://doi.org/10.1039/C7IB00022G
Dokukina IV, Gracheva ME (2010) A model of fibroblast motility on substrates with different rigidities. Biophys J 98:2794–2803. https://doi.org/10.1016/j.bpj.2010.03.026
Doyle PS, Shaqfeh ESG, Gast AP (1997) Dynamic simulation of freely draining flexible polymers in steady linear flows. J Fluid Mech 334:251–291. https://doi.org/10.1017/S0022112096004302
Drasdo D, Hoehme S (2012) Modeling the impact of granular embedding media, and pulling versus pushing cells on growing cell clones. New J Phys. https://doi.org/10.1088/1367-2630/14/5/055026
Elosegui-Artola A, Bazellières E, Allen MD et al (2014) Rigidity sensing and adaptation through regulation of integrin types. Nat Mater 13:631–7. https://doi.org/10.1038/nmat3960
Elosegui-Artola A, Oria R, Chen Y et al (2016) Mechanical regulation of a molecular clutch defines force transmission and transduction in response to matrix rigidity. Nat Cell Biol 18:540–548. https://doi.org/10.1038/ncb3336
Escribano J, Sánchez MT, García-Aznar JM (2014) A discrete approach for modeling cell-matrix adhesions. Comput Part Mech 1:117–130. https://doi.org/10.1007/s40571-014-0006-7
Escribano J, Sanchez MT, Garcıa-Aznar JM (2015) Modeling the formation of cell-matrix adhesions in 3D matrices. J Theor Biol 384:84–94. https://doi.org/10.1016/j.jtbi.2015.07.015
Gardel ML, Sabass B, Ji L et al (2008) Traction stress in focal adhesions correlates biphasically with actin retrograde fl ow speed. J Cell Biol 183:999–1005. https://doi.org/10.1083/jcb.200810060
Gonzalez-Valverde I, Garcia-Aznar JM (2017) A hybrid computational model to explore the topological characteristics of epithelial tissues. Int J Numer Method Biomed Eng. https://doi.org/10.1002/cnm.2877
Haeger A, Wolf K, Zegers MM, Friedl P (2015) Collective cell migration: guidance principles and hierarchies. Trends Cell Biol 25:556–566. https://doi.org/10.1016/j.tcb.2015.06.003
Hartman CD, Isenberg BC, Chua SG, Wong JY (2016) Vascular smooth muscle cell durotaxis depends on extracellular matrix composition. Proc Natl Acad Sci U S A 113:11190–11195. https://doi.org/10.1073/pnas.1611324113
Hughes TJR (1987) The finite element method: linear static and dynamic finite element analysis, vol 825. Prentice-Hall, Inc, Englewood Cliffs
Hughes TJR (2012) The finite element method: linear static and dynamic finite element analysis. Courier Corporation, North Chelmsford
Jia D, Jolly MK, Boareto M et al (2015) OVOL guides the epithelial-hybrid-mesenchymal transition. Oncotarget 6:15436–15448. https://doi.org/10.18632/oncotarget.3623
Kabla AJ (2012) Collective cell migration: leadership, invasion and segregation. J R Soc Interface 9(77):3268–3278. https://doi.org/10.1098/rsif.2012.0448
Kanchanawong P, Shtengel G, Pasapera AM et al (2010) Nanoscale architecture of integrin-based cell adhesions. Nature 468:580–4. https://doi.org/10.1038/nature09621
Kim T, Hwang W, Kamm RD (2007) Computational analysis of a cross-linked actin-like network. Exp Mech 49:91–104
Kim MC, Whisler J, Silberberg YR et al (2015) Cell invasion dynamics into a three dimensional extracellular matrix fibre network. PLoS Comput Biol 11:1–29. https://doi.org/10.1371/journal.pcbi.1004535
Kong F, García AJ, Mould aP et al (2009) Demonstration of catch bonds between an integrin and its ligand. J Cell Biol 185:1275–84. https://doi.org/10.1083/jcb.200810002
Kulawiak DA, Camley BA, Rappel W-J (2016) Modeling contact inhibition of locomotion of colliding cells migrating on micropatterned substrates. PLoS Comput Biol 12(12):1–25. https://doi.org/10.1371/journal.pcbi.1005239
Lang NR, Skodzek K, Hurst S et al (2015) Biphasic response of cell invasion to matrix stiffness in three-dimensional biopolymer networks. Acta Biomater 13:61–67. https://doi.org/10.1016/j.actbio.2014.11.003
Leong FY (2013) Physical explanation of coupled cell-cell rotational behavior and interfacial morphology: a particle dynamics model. Biophys J 105:2301–2311. https://doi.org/10.1016/j.bpj.2013.09.051
Lin S-Z, Li B, Xu G-K, Feng X-Q (2016) Collective dynamics of cancer cells confined in a confluent monolayer of normal cells. J Biomech 52:140–147. https://doi.org/10.1016/j.jbiomech.2016.12.035
Liu F, Mih JD, Shea BS et al (2010) Feedback amplification of fibrosis through matrix stiffening and COX-2 suppression. J Cell Biol 190:693–706. https://doi.org/10.1083/jcb.201004082
Majumdar R, Sixt M, Parent CA (2014) New paradigms in the establishment and maintenance of gradients during directed cell migration. Curr Opin Cell Biol 30:33–40. https://doi.org/10.1016/j.ceb.2014.05.010
Malet-Engra G, Yu W, Oldani A et al (2015) Collective cell motility promotes chemotactic prowess and resistance to chemorepulsion. Curr Biol 25:242–250. https://doi.org/10.1016/j.cub.2014.11.030
Martin P (1997) Wound healing-aiming for perfect skin regeneration. Science 276:75–81. https://doi.org/10.1126/science.276.5309.75
Mayor R, Carmona-Fontaine C (2010) Keeping in touch with contact inhibition of locomotion. Trends Cell Biol 20:319–328. https://doi.org/10.1016/j.tcb.2010.03.005
Méhes E, Vicsek T (2014) Collective motion of cells: from experiments to models. Integr Biol 6:831–854. https://doi.org/10.1039/C4IB00115J

Merkher Y, Weihs D (2017) Proximity of metastatic cells enhances their mechanobiological invasiveness. Ann Biomed Eng 45(6):1399–1406. https://doi.org/10.1007/s10439-017-1814-8

Moreno-Arotzena O, Borau C, Movilla N et al (2015) Fibroblast migration in 3D is controlled by haptotaxis in a non-muscle myosin II-dependent manner. Ann Biomed Eng 43:3025–3039. https://doi.org/10.1007/s10439-015-1343-2

Movilla N, Borau C, Valero C, García-Aznar JM (2017) Degradation of extracellular matrix regulates osteoblast migration: a microfluidic-based study. Bone 107:10–17. https://doi.org/10.1016/j.bone.2017.10.025

Novikova EA, Storm C (2013) Contractile fibers and catch-bond clusters: a biological force sensor? Biophys J 105:1336–45. https://doi.org/10.1016/j.bpj.2013.07.039

Novikova EA, Raab M, Discher DE, Storm C (2017) Persistence-driven durotaxis: generic, directed motility in rigidity gradients. Phys Rev Lett 118:1–5. https://doi.org/10.1103/PhysRevLett.118.078103

Peng L, Trucu D, Lin P, Thompson A, Chaplain MAJ (2017) A multiscale mathematical model of tumour invasive growth. Bull Math Biol 79(3):389–429. https://doi.org/10.1007/s11538-016-0237-2

Plotnikov SV, Pasapera AM, Sabass B, Waterman CM (2012) Force fluctuations within focal adhesions mediate ECM-rigidity sensing to guide directed cell migration. Cell 151:1513–1527. https://doi.org/10.1038/jid.2014.371

Reina-Romo E, Gómez-Benito MJ, García-Aznar JM et al (2010) Growth mixture model of distraction osteogenesis: effect of pretraction stresses. Biomech Model Mechanobiol 9:103–115. https://doi.org/10.1007/s10237-009-0162-5

Roca-Cusachs P, Sunyer R, Trepat X (2013) Mechanical guidance of cell migration: lessons from chemotaxis. Curr Opin Cell Biol 25:543–549. https://doi.org/10.1016/j.ceb.2013.04.010

Rodriguez EK, Hoger A, McCulloch AD (1994) Stress-dependent finite growth in soft elastic tissues. J Biomech 27:455–467. https://doi.org/10.1016/0021-9290(94)90021-3

Rørth P (2011) Whence directionality: guidance mechanisms in solitary and collective cell migration. Dev Cell 20:9–18. https://doi.org/10.1016/j.devcel.2010.12.014

Sepúlveda N, Petitjean L, Cochet O et al (2013) Collective cell motion in an epithelial sheet can be quantitatively described by a stochastic interacting particle model. PLoS Comput Biol 9:e1002944. https://doi.org/10.1371/journal.pcbi.1002944

Singh SP, Schwartz MP, Lee JY et al (2014) A peptide functionalized poly (ethylene glycol) (PEG) hydrogel for investigating the influence of biochemical and biophysical matrix properties on tumor cell migration. Biomater Sci 2:1024. https://doi.org/10.1039/c4bm00022f

Stefanoni F, Ventre M, Mollica F, Netti PA (2011) A numerical model for durotaxis. J Theor Biol 280:150–158. https://doi.org/10.1016/j.jtbi.2011.04.001

Sunyer R, Conte V, Escribano J et al (2016) Collective cell durotaxis emerges from long-range intercellular force transmission. Science 353:1157–1161. https://doi.org/10.5061/dryad.r8h3n

Tambe DT, Corey Hardin C, Angelini TE et al (2011) Collective cell guidance by cooperative intercellular forces. Nat Mater 10:469–475. https://doi.org/10.1038/nmat3025

Theveneau E, Marchant L, Kuriyama S et al (2010) Collective chemotaxis requires contact-dependent cell polarity. Dev Cell 19:39–53. https://doi.org/10.1016/j.devcel.2010.06.012

Ulrich TA, De Juan Pardo EM, Kumar S (2009) The mechanical rigidity of the extracellular matrix regulates the structure, motility, and proliferation of glioma cells. Cancer Res 69:4167–4174. https://doi.org/10.1158/0008-5472.CAN-08-4859

Vermolen FJ, van der Meijden RP, Van Es M et al (2015) Towards a mathematical formalism for semi-stochastic cell-level computational modeling of tumor initiation. Ann Biomed Eng 43:1680–1694. https://doi.org/10.1007/s10439-015-1271-1

Vermolen FJ, Arkesteijn ECMM, Gefen A (2016) Modelling the immune system response to epithelial wound infections. J Theor Biol 393:158–169. https://doi.org/10.1016/j.jtbi.2015.12.030

Wolfenson H, Meacci G, Liu S et al (2016) Tropomyosin controls sarcomere-like contractions for rigidity sensing and suppressing growth on soft matrices. Nat Cell Biol 18:33–42. https://doi.org/10.1038/ncb3277

Yang J, Weinberg RA (2008) Epithelial-mesenchymal transition: at the crossroads of development and tumor metastasis. Dev Cell 14:818–829. https://doi.org/10.1016/j.devcel.2008.05.009

Yu G, Feng J, Man H, Levine H (2017) Phenomenological modeling of durotaxis. Phys Rev E 96(1):1–6. https://doi.org/10.1103/PhysRevE.96.010402